



Hidden Affinities Between Electric and Acoustic Activities in Brittle Materials at Near-Fracture Load Levels

D. Triantis¹ · E. D. Pasiou² · I. Stavrakas¹ · S. K. Kourkoulis²

Received: 24 March 2020 / Accepted: 8 November 2021 / Published online: 12 January 2022
© The Author(s), under exclusive licence to Springer-Verlag GmbH Austria, part of Springer Nature 2021

Abstract

The time evolution of the electric activity in brittle materials, mechanically loaded at levels approaching the ones causing catastrophic fracture, is studied and modeled in terms of the time-to-failure parameter. The electric activity is considered in juxtaposition to the respective acoustic one. The latter was analytically described in a recently published paper in terms of the F-function. The comparison is implemented to calibrate the outcomes of the Pressure-Stimulated Currents technique by means of the respective ones of a mature sensing technique, i.e., that of the Acoustic Emissions. Moreover, this comparative study aims to reveal possible common qualitative features of these sensing techniques. Using data from three different experimental protocols quite a few hidden affinities between the acoustic and electric signals recorded are revealed. Especially at the very last loading stages, i.e., while macroscopic fracture is impending, the time evolution of both the electric and acoustic emissions is governed by a power law, the exponent of which varies in a relatively narrow interval around unity. Moreover, it is shown that both techniques provide interesting pre-failure indicators, warning about upcoming fracture. At least for some protocols of the present study, it is concluded that the pre-failure indicators of the electric signals precede the respective ones of the acoustic signals. The combined use of data obtained from completely different loading schemes, materials, types of specimens and load application modes offers reliable support to the conclusions drawn while at the same time guarantees their wide applicability.

Keywords Electric emissions · Pressure-Stimulated Currents · Acoustic emissions · F-function · Cement mortar · Dionysos marble · Compression · Three-point bending · Double-edge notched specimens

1 Introduction

It is nowadays widely accepted that during the deformation of solid materials, a variety of mechanisms are activated generating, among others, electric signals. These mechanisms are closely related to the development and propagation of cracks at various length scales (Enomoto and Hashimoto 1990; Ogawa and Miura 1985; Vallianatos et al. 2004). In this context, the study of fracture of inhomogeneous

materials in conjunction with the respective transient electric phenomena has recently attracted the interest of the scientific community. This interest is further intensified since reliable indications exist that upcoming macroscopic fracture is related to an intense increase of the magnitude of the electric signals emitted (Stavrakas et al. 2003).

The underlying phenomenon, responsible for the generation of these electric signals, is associated with the fact that micro-cracking is the origin of motion of electric charges and consequently changes of local polarizations. Indeed, during cracking ionic bonds break polarizing the newly formed crack edges creating, thus, electric dipoles. The existence of these dipoles is, in turn, responsible for an electric potential across the crack allowing a current to flow. Under specific conditions, this electric current is detectable, not only during laboratory-scale experiments (Cartwright et al. 2014; Stavrakas et al. 2003) but, also, at geodynamic scales (Varotsos 2005). Series of recently published experimental studies attempt to shed light on the relation between

✉ S. K. Kourkoulis
stakkour@central.ntua.gr

¹ Department of Electrical and Electronics Eng., Laboratory of Electronic Devices and Materials, University of West Attica, 122 10 Athens, Greece

² Department of Mechanics, Laboratory for Testing and Materials, National Technical University of Athens, Theocaris Building, Zografou Campus, 157 73 Athens, Greece

these electric signals and the damage mechanisms activated during loading, for specimens made of either dry or saturated minerals and rocks (Archer et al. 2016; Fursa et al. 2019; Li et al. 2015; Stavrakas et al. 2004; Triantis et al. 2008; Yoshida et al. 1997). A short discussion on the models developed to enlighten the mechanisms responsible for the generation of these weak electric currents can be found in Sect. 4 (Discussion).

Concerning the techniques used for the detection and recording of these electric signals, the most widely adopted one is that of the Pressure-Stimulated Currents (PSCs) (Triantis et al. 2006a, b), which has been widely applied for the detection of electric emissions during mechanical loading and damage of brittle building materials, either natural or artificial. According to this technique, the electric signal is detected as an extremely weak electric current using sensitive electrometers. The detecting sensors are gold-plated electrodes properly attached at strategic points of the loaded specimens. It is to be mentioned here, that the term PSC was initially used in the literature to describe the emission of a transient electric signal (polarization or depolarization), as a result of gradual variation of the mechanical stress induced on solids containing electric dipoles due to various types of defects (Varotsos et al. 1998).

Regarding the advantages of the PSC technique, one should mention the very low cost of the sensors and the devices required for its application, the easy preparation of the experimental setup, and the fact that its application does not influence the stress and strain fields developed during loading. Of increased importance is, also, the fact that a long series of laboratory experiments on rock-like materials (such as marble and amphibolite) indicated that the PSC recorded increases significantly when the load induced approaches its critical value, i.e., the value causing macroscopic collapse (Kourkoulis et al. 2018; Kyriazopoulos et al. 2011; Pasiou and Triantis 2017). In other words, the PSC technique provides well distinguishable pre-failure indicators, and therefore, it could potentially become a flexible tool for Structural Health Monitoring purposes.

Nowadays, the PSC technique is widely used worldwide, either according to its original form (Cartwright et al. 2014; Li et al. 2015) or by adopting alternative procedures based on similar underlying principles (Aydin et al. 2009; Fursa et al. 2017; Sharma et al. 2018).

The data provided by the PSC technique have been recently considered in juxtaposition to the respective ones provided by the Acoustic Emissions (AE) technique, both for calibration and validation reasons (Kourkoulis et al. 2018; Pasiou and Triantis 2017). The reason for this choice is that the AE technique is perhaps the most mature, well established, and widely used non-destructive sensing technique for monitoring the damage processes within loaded structural elements made of either natural or artificial building

materials. The acoustic emission is a natural phenomenon according to which mechanical energy is released in the form of spherical stress waves, during the activation of damage mechanisms. The basic principles of the AE technique are thoroughly described in the literature (Aggelis 2013; Eitzen and Wadley 1984; Ishida et al. 2017; Ohtsu 2010) and it is nowadays considered a unique tool for the study of internal damage mechanisms as well as for Structural Health Monitoring of either individual structural elements or whole structures. A variety of characteristics of the AEs detected and recorded during loading (e.g., the number of acoustic events, the number of acoustic hits, the amplitude and the rise time of the acoustic signals, the frequency of acoustic events, etc.), closely related to the stress state and the damage level of the loaded sample, are used for the above purposes, depending on the specific target of each study.

Following previous studies of the authors' team, a parallel assessment of experimental data provided by both the AE- and the PSC-techniques is here undertaken, aiming to reveal possible qualitative correlations between the acoustic and the electric activities. For a more enlightening representation of the time evolution of the acoustic activity, a recently introduced procedure is adopted, based on the F-function, i.e., the time function expressing the average frequency of the generation of AE hits, in terms of the inter-event time intervals, in a sliding time window of N consecutive hits (Triantis and Kourkoulis 2018).

2 Experimental Protocols: Materials, Specimens, Loading Schemes, and Experimental Setups

Two brittle materials were used for the construction of the specimens: cement mortar and Dionysos marble. The cement-mortar specimens were prepared using ordinary Portland cement, sand of fine aggregates and water at a ratio of 1:3:0.5, respectively. The size of the fine aggregates was relatively small, ranging from approximately 0.6 mm to about 1.8 mm, thus resulting to specimens of relatively low heterogeneity. Concerning Dionysos marble (the natural building stone extensively used for the restoration project, in progress, of the Athenian Acropolis), its composition and its mechanical properties are well documented in the literature (Exadaktylos et al. 2001; Kourkoulis et al. 1999; Vardoulakis et al. 1998).

In this study, data from three different experimental protocols will be considered. During the first one, prismatic specimens, made of either cement mortar or Dionysos marble, were loaded under uniaxial monotonic compression until fracture. The cement-mortar specimens were of square cross-section ($50 \times 50 \text{ mm}^2$) and their height was equal to 70 mm. The standardized procedure was followed

to cure these specimens before they were tested. More specifically, they were cured in a room with constant ambient temperature of about 22 °C and 75–80% humidity for at least 28 days to reach 90–95% of their strength. The marble specimens were, also, of square cross-section ($40 \times 40 \text{ mm}^2$) and their height was equal to 100 mm. The load was applied along the strong anisotropy direction of Dionysos marble, i.e., normally to the material layers (Kourkoulis et al. 1999). Both types of specimens were loaded under stress-controlled conditions at a rate equal to about 0.30 MPa/s, thus simulating quasi-static loading conditions. An electric strain gauge was attached on one of the lateral surfaces of the specimens to measure the axial strain developed (Fig. 1a). Moreover, one acoustic sensor R15 α was properly coupled, using silicone, on the lateral surface opposite to that on which the strain gauge was glued. A preamplifier (Mistras Group, Inc.) with 40 dB gain was used (the acquisition system used in all experiments was the PCI-2). The 40 dB threshold was chosen, according to the data of a series of preliminary acquisitions, to avoid recording the background noise. Finally, for the detection of the PSC signal, a pair of electrodes was attached on the remaining two lateral surfaces of the specimens (Fig. 1a). In this direction, a thin layer of conductive silver paste was initially smeared on the specimens, at the points where the electrodes were to be attached. Then, the electrodes were placed on the silver paste and they were kept in place using a suitable spring. The same procedure was followed for the second and third protocols described in next paragraphs. The only difference is that in the third protocol suitable patches were used instead of springs. A sensitive programmable electrometer (Keithley, 6517A), resolving currents between 0.1 fA and 20 mA in 11 ranges, was used to record the electric signals. It is here underlined that thin PTFE (Teflon) sheets were interposed between the specimens' bases and the loading platens for the specimen's electrical isolation and also for the minimization of friction.

Before proceeding to the description of the remaining two experimental protocols, it is necessary to mention a few things about the electrical isolation and shielding aspects. Indeed, according to commercially available tables, the electrical resistivity of PTFE is of the order of 10^{12} – $10^{17} \Omega\text{m}$ while for marble it is only equal to about $10^8 \Omega\text{m}$. Moreover, during the tests and for the whole duration of each experimental procedure, all mechanical parts (including the loading frame) are connected to the ground, for electrical noise affecting the measurements to be eliminated. Electrical ground is also applied to the plates that directly contact the PTFE interface to the specimen. Under the above measures, it is believed that PTFE cannot be polarized and produce any electrical field in the specimen's body. In addition, it is mentioned that initially all experiments were conducted in a Faraday cage (shield) ensuring that EM noise would have no impact on the recorded PSCs. Since then, several tests

were conducted to evaluate the above-specified impact. It was observed that the recorded PSC was not different when the Faraday shield was removed. In any case, the sensitive electrometers used record the electrical current long before the experimental apparatus is activated thus quantifying any background noise. For all three protocols described here, the background PSC was low enough and can be considered negligible.

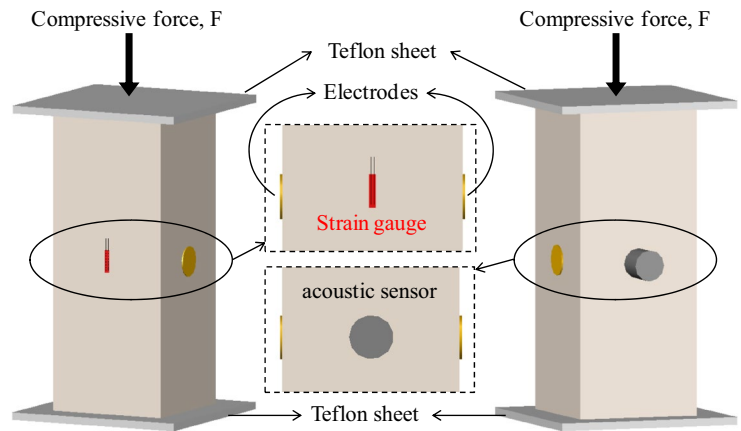
Special attention was paid during the experiments to the “clock” synchronizing issue. For all experiments of all three protocols described in this study, the equipment of the AE- and PSC-techniques started recording at the same time instant. For most accurate synchronization, the outcome of the applied load channel was continuously recorded not only by the internal system of the loading frame but also by both the AE and PSC computers. In this context, it should be kept in mind that from the AE sensor (R15 α by Mistras Group, Inc.), the signal captured is amplified in its analogue state and transferred to the PCI-2 in analogue mode. The PCI-2 module is a 2-channel data acquisition and digital signal processing system on a single full-size 32-bit PCI-Card. Moreover, it is here highlighted that the load cell, attached on the loading frame, has three (3) analogue voltage outputs. The output voltage corresponds to the value of the applied load. These outputs are isolated between each other not to be affected by any A/D external measuring system. These outputs are sent to: (1) Extra analogue input of the PCI-2 module and to (2) analogue input of the PSC system that is the National Instruments PCI-MIO-16E with the CB-68LP input interface. The software used for the PSC is the Keysight-Vee while for the AE the AEWIn (by Physical Acoustics corp.) gets the load values directly from the loading frame.

It should be, also, kept in mind that there is no interaction between the AE and PSC measurements before the end of each experiment. The AE and PSC data are analyzed only after the experiment. The common signal that is shared (through the above-mentioned procedure) between the two measuring systems is the analogue voltage that corresponds to the applied mechanical load. Finally, the electrometer used to record the PSCs is the Keithley 6517A, connected to the PC through the National Instruments GPIB-488.

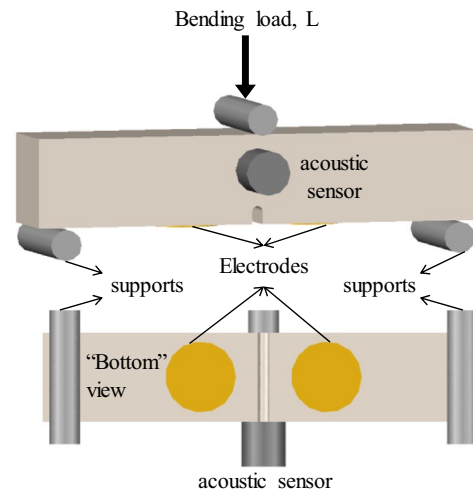
The “clocks” of AE and PSC were finally synchronized by putting the waveforms of each load data together. The sampling interval of the PSC is set to 0.1 s to let the system achieve its maximum sampling rate. The procedure of sampling is through polling between the PSC values and load. The maximum sampling interval the system achieved in this case is approximately equal to 0.4 s.

The second experimental protocol included three-point bending (3PB) tests, with beam-shaped specimens (made of the same as above cement mortar and Dionysos marble), monotonically loaded until fracture. The cement-mortar beams were of square cross-section ($50 \times 50 \text{ mm}^2$) and

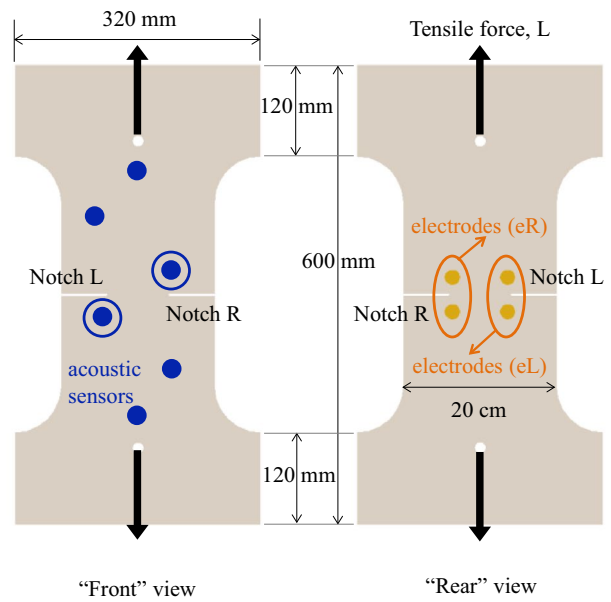
Fig. 1 Schematic representation of the experimental setup of the: **a** uniaxial compression; **b** three-point bending and **c** direct tension, experimental protocols



(a)



(b)



(c)

their length was equal to 200 mm. Load-control conditions were adopted at a rate equal to about 45 N/s, ensuring again quasi-static loading scheme. The marble beams were, also, of square cross-section ($20 \times 20 \text{ mm}^2$) while their length was equal to 100 mm. Displacement-control conditions were adopted, at a constant rate equal to $0.08 \text{ } \mu\text{m/s}$, simulating again quasi-static loading conditions. The cement-mortar beams were tested intact, i.e., they were not notched. On the contrary, the marble beams were mechanically notched at their middle section. The depth of the notch was equal to 4 mm while its width was equal to 1.5 mm. For both cases, the detection and recording of the PSC and the AEs was implemented using the experimental setup described in the first experimental protocol, as it is shown in Fig. 1b.

Concerning the third experimental protocol, double-edge notched tensile specimens (Fig. 1c), made of Dionysos marble, were tested. The thickness of the specimens was 12 mm. Their geometry and dimensions are shown in Fig. 1c. Two symmetrical notches were mechanically machined at both sides of the specimens. The depth of the notches was equal to $a=60 \text{ mm}$ while their width was equal to 1.5 mm. Two R15 α piezoelectric acoustic sensors (denoted as chR and chL), similar to the ones used in the previous two protocols, were properly mounted in the immediate vicinity of the crowns of the notches at the front side of the specimens (Fig. 1c). For the detection of the PSC, two pairs of cyclically shaped electrical contacts (denoted as eR and eL), made of copper, were attached on the rear side of the specimens, again in the immediate vicinity of the crowns of the two notches (Fig. 1c). Displacement-control conditions were adopted, at a constant rate equal to about $3 \text{ } \mu\text{m/s}$, ensuring, again, a quasi-static loading scheme.

It is here clarified that the data provided by the AE technique have been already discussed and analyzed in terms of the F-function by Loukidis et al. (2021). However, for the sake of completeness of the present paper and to make a direct comparison between the data provided by the PSC technique and those provided by the AE one easier, the respective data for the time evolution of the F-function are briefly summarized, also, in this manuscript, in the respective sections.

3 Experimental Results

3.1 Uniaxial Compression of Cement-Mortar and Marble Specimens

Data from two representative tests (one with specimen made of cement mortar and one with specimen made of marble) are analyzed in this section. During loading the axial stress, the axial strain, the PSC and the acoustic hits with amplitude exceeding 40 dB were recorded and stored. The overall number of acoustic hits recorded for the cement-mortar specimen was $n=1780$ while that for the marble specimen was $n=1189$.

The time evolution of the axial strain, for both tests is plotted in Fig. 2a. The respective axial stress–axial strain curves are plotted in Fig. 2b. Both materials are characterized by an almost linear response, excluding the very early loading stages (due to inevitable bedding errors characterizing the compression tests), and also, the loading stages just before fracture (due to the development of non-reversible phenomena preceding the final macroscopic fracture). The elastic modulus for the cement-mortar specimen is 20 GPa

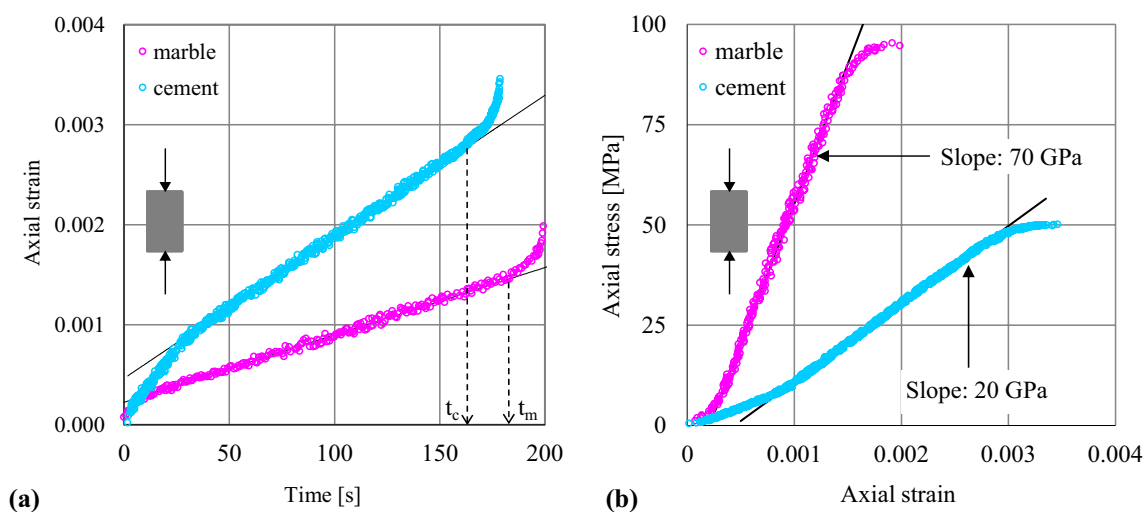


Fig. 2 **a** Time evolution of the axial strain and **b** the axial stress versus axial strain, for typical tests of the uniaxial compression protocol with cement-mortar and marble specimens

and that for the marble one 70 GPa. Deviation from linearity was observed at a time instant equal to about $t_c = 165$ s for the cement-mortar specimen and about $t_m = 180$ s for the marble one. Fracture occurred at time instants equal to about 179 and 199 s, respectively (corresponding to the time instants at which a saturated AE hit of 99 dB was recorded).

The time evolution of the PSCs recorded during these two tests is plotted in Fig. 3, along semi-logarithmic scale, in juxtaposition to the respective evolution of the axial strain. It is observed that the electric activity in the cement-mortar specimen is significantly stronger compared to the respective one in the marble specimen. Indeed, the PSC in the cement-mortar specimen attains values approaching the order of nA, in excellent agreement with previously published results (Triantis et al. 2012). The difference of the magnitude of the recorded PSCs is attributed to the fact that cement mortar favors charge and dipole creation and propagation due to its chemical composition and pre-existing ionic content. Similar conclusions concerning the difference between the PSC level in cement-based and marble specimens are mentioned in the literature [see, for example, the papers by Triantis et al. (2006b, 2012)]. On the other hand, marble has low quartz content (preventing piezoelectric behavior) and porosity (preventing electrokinetic effects) while its chemical composition is not favoring large dipole movements and consequent significant electrical current flow. Indeed, especially for Dionysos marble, its content in quartz is very low, about 0.2% (its density is about 2.7 g/cm^3 and its porosity is approximately equal to about 0.4%). The physical properties and characteristics of Dionysos marble (which is mainly composed of calcite (98%) and other minerals such as muscovite, sericite and chlorite) can be found in relative studies by Kleftakis et al. (2000) and Vardoulakis et al. (1998).

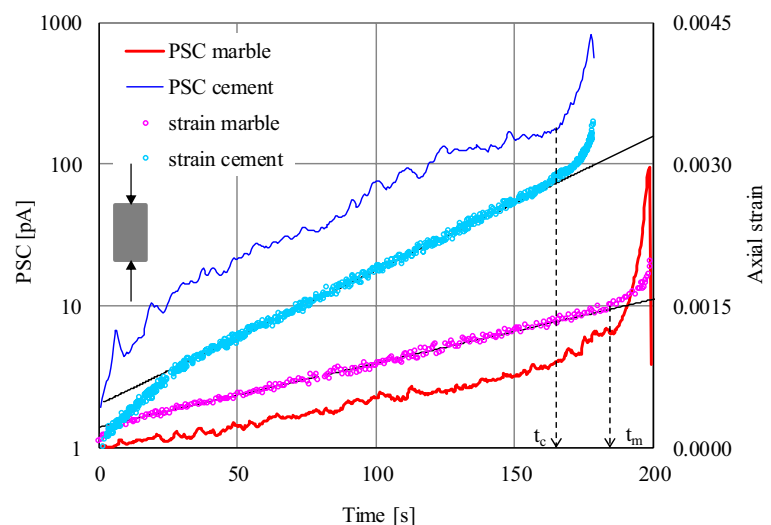
It is worth mentioning that the rate of increase of the PSC changes drastically and the PSC values start increasing much

more abruptly at the times instants t_m and t_c , mentioned previously as the time instants at which deviation from linearity is observed. Moreover, it is noticed that the PSC attains its peak values about 1 s before the macroscopic fracture of the specimens (recall that the actual sampling rate for the PSC is 2.5 samples/s). It is well documented (Stavarakas et al. 2003; Vallianatos et al. 2004) that this peak of the PSC designates the onset of unstable crack propagation. In addition, the decrease of the PSC values observed in both tests (practically during the very last second of the loading procedure) is justified due to the development of macro-cracks, which, in turn, reduce drastically the electric paths within the mass of the specimen and more specifically along the direction defined by the two electrodes recording the PSC signals. The specific phenomenon, i.e., the abrupt decrease of the PSC values just before macroscopic fracture, is, also, well documented in the relative literature (Triantis et al. 2008).

For the acoustic activity to be studied by means of the rate of generation of acoustic hits, an alternative, recently proposed technique, based on the F-function (Triantis and Kourkoulis 2018) is here employed, instead of the traditional procedure based on the “number-of-hits-per-second” parameter. The specific procedure has been already used by a number of researches worldwide (Niu 2019; Wang et al. 2019; Zhang et al. 2019). The F-function represents the average frequency of appearance of AE hits in a sliding time window of N consecutive AE hits, in terms of the inter-event time intervals. The potential influence of the numerical value of N on the conclusions drawn is discussed in Sect. 5 (Concluding remarks).

For the two tests analyzed here, the F-function was calculated using a value equal to $N=50$, i.e., making use of the inter-event time intervals of 50 successive AE hits. The inverse of the average value of the respective inter-event time intervals of each group of N successive AE hits is

Fig. 3 The PSC recorded during two typical tests with cement-mortar and marble specimens of the uniaxial compression protocol in juxtaposition to the respective axial strain developed



paired to the mean value, τ , of the time instants $t_i, i = 1 \dots N$, at which each one of the N AE hits of the group is recorded (Triantis and Kourkoulis 2018; Triantis et al. 2020). It is here emphasized that τ is an average time instant. By sliding the window of the N consecutive hits, with a step equal to one AE hit, the function $F(\tau)$ is obtained.

It has been pointed out that plotting the F-function in terms of the time-to-failure parameter (i.e., the difference $(t_f - \tau)$, where t_f corresponds to the time instant at which fracture occurs) using logarithmic scales, enlightens critical details of the time evolution of the acoustic activity at the stages just before macroscopic fracture (Triantis and Kourkoulis 2018). In this context, the F-function for the cement-mortar specimen is plotted in Fig. 4a, against the $(t_f - \tau)$ parameter. In the same figure, the time evolution of the respective PSC is, also, plotted against the $(t_f - t)$ parameter, for comparison reasons. It is to be emphasized that the intensive increase of both the acoustic activity (in terms of the F-function) and, also, of the PSC values, starts almost 14 s before macroscopic fracture. Combining this observation with the respective one concerning the deviation from linearity of the mechanical response of the specific specimen at the time instant with $t_c = 165$ s (see Fig. 2a) and noting that $(t_f - t_c) = 14$ s, it is concluded that the acoustic activity is strongly intensified when the mechanical response of the material abandons linearity. In other words, the intensification of the acoustic activity is closely related to the onset of generation of non-reversible phenomena within the mass of the specimen tested.

From Fig. 4a, an excellent qualitative agreement between the time evolution of the F-function and that of the respective PSC values is deduced, indicating that the strong intensification of the electric activity, observed a little before macroscopic fracture occurs, is, also, strongly related to the activation of mechanisms generating non-reversible phenomena within the material loaded.

For the time interval of steep increase of the acoustic and the electric activity, the time evolution of both the F-function and the PSC is described by empirical power laws of the form:

$$F(\tau) = A_1 \cdot (t_f - \tau)^{-m_1} \tag{1}$$

and

$$PSC(t) = A_2 \cdot (t_f - t)^{-m_2} \tag{2}$$

where A_1 and A_2 are constants. The exponents m_1 and m_2 can be interpreted as representing the intensity of increase of the F-function and the PSC, respectively. For the specific tests, best fitting procedure provides for the exponents m_1 and m_2 values equal to $m_1 = 0.84$ for the F-function and for the PSC to $m_2 = 0.71$. It is here mentioned that for both cases (and for all fitting procedures described in this and, also, in

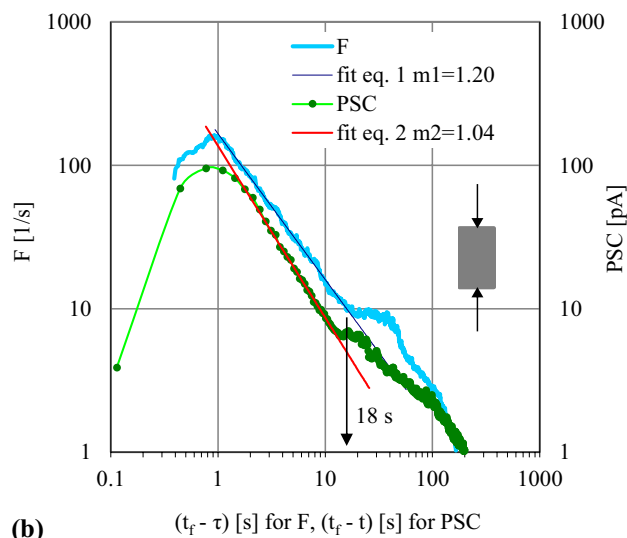
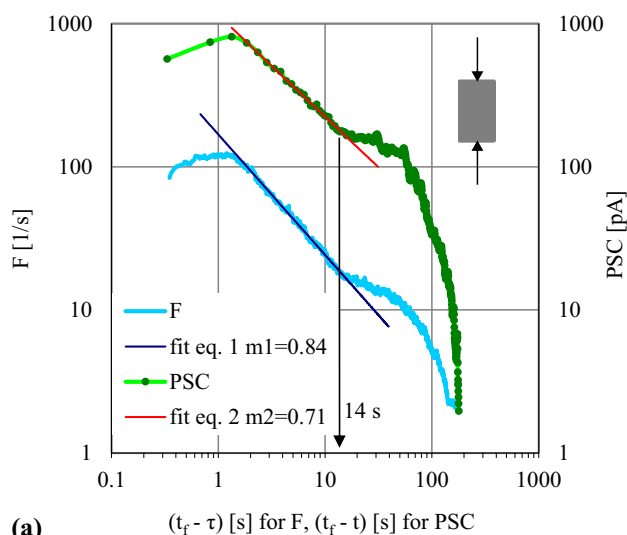


Fig. 4 The PSC and the F-function in terms of the time-to-failure parameter along logarithmic scales for a **a** cement-mortar and **b** marble specimen, under uniaxial compression

the next sections), the regression coefficients varied in the interval (0.98–0.99).

Both the PSC and the F-function attain their maximum values 1 s before the macroscopic fracture. The maximization of the F-function and its dramatic reduce that follows can be explained taking into account that during this very last time interval of the loading procedure AEs of increased amplitude and duration are generated and, in turn, their inter-event time intervals are characterized by increased values. As a result, the F-function, which is the inverse of the average value of the inter-event times starts decreasing.

The conclusions drawn for the cement-mortar specimen are in excellent agreement with the respective observations for the Dionysos marble specimen, as it can be seen

in Fig. 4b, in which the same quantities as those in Fig. 4a are plotted. The power laws of Eqs. (1) and (2), describing the intensive increase of the F-function and the PSC, are now valid for the time interval starting at about 18 s before macroscopic fracture, again in excellent agreement with the time instant at which the marble specimen abandons its linear response (which according to Fig. 2a corresponds to the time instant with $(t_f - t_m) \sim 19$ s). For this test, best fitting procedure provides values for the m_1 and m_2 exponents equal to $m_1 = 1.20$ and $m_2 = 1.04$, for the F-function and the PSC, respectively. It is thus again concluded that the onset of strong intensification of both the acoustic and electric activity, a little before the macroscopic fracture of the specimen, is closely related to the onset of generation of non-reversible phenomena.

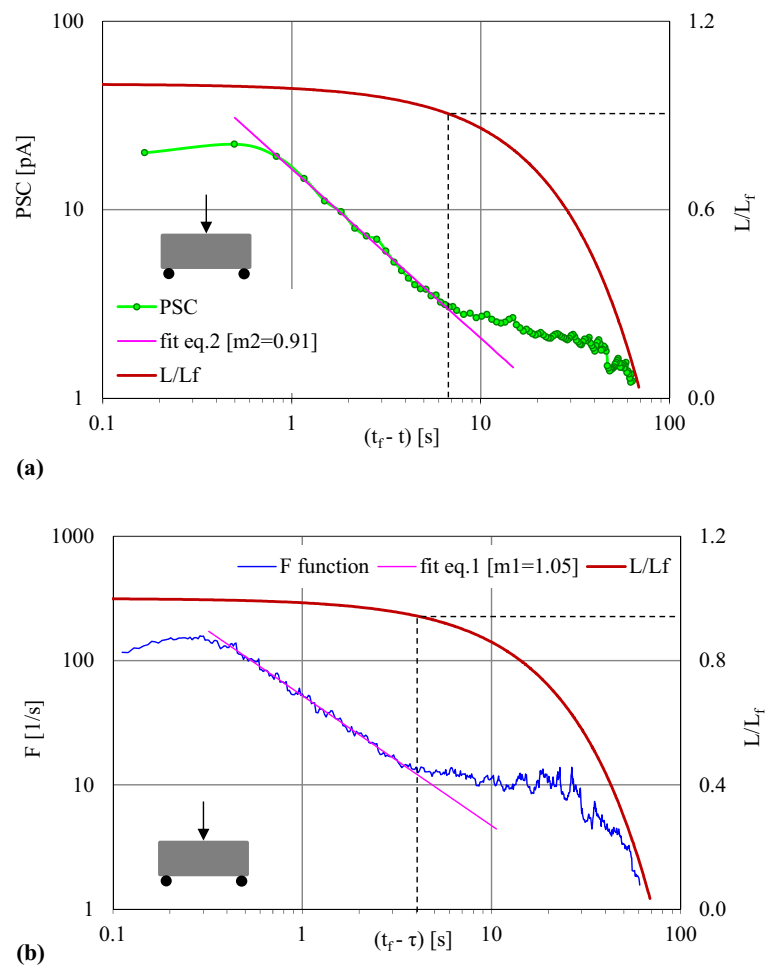
3.2 Three-Point Bending (3PB) of Cement-Mortar and Marble Beams

The time evolution of the PSC for a representative 3PB test with an intact cement-mortar beam is plotted in Fig. 5a. In the same figure, the respective evolution of the externally

applied force L is plotted, normalized over its maximum value, L_f , which for the specific test analyzed here was equal to $L_f = 3.25$ kN. It is interesting to note that the steep increase of the PSC starts at $(t_f - t) \sim 7$ s, i.e., 7 s before macroscopic fracture. At the specific time instant, the load level is equal to about 90% of the respective ultimate value. Moreover, it is to be highlighted that the phase of intensively increasing electric activity is, again, governed by the power law of Eq. (2) and the value of exponent m_2 providing best fit is equal to $m_2 = 0.91$.

Concerning the acoustic activity in the as above cement-mortar specimen, the number of acoustic hits (of amplitude exceeding 40 dB) recorded, was equal to $n = 580$. The acoustic activity is, again, described in terms of the F-function, however, the number of successive hits of the sliding window was now set equal to $N = 25$. The time evolution of the F-function against the $(t_f - \tau)$ parameter is plotted along logarithmic scales in Fig. 5b, following the way Fig. 5a was drawn. It is seen from Fig. 5b that the acoustic activity becomes intensive after a time instant equal to about $(t_f - \tau) = 4$ s or equivalently at a load level exceeding 95% of the fracture force. It is here recalled that the time parameter

Fig. 5 The **a** PSC and **b** F-function in terms of the time-to-failure parameter along logarithmic scales for a representative specimen made of cement mortar under three-point bending, in juxtaposition to the normalized load induced



τ (average of the time instants at which the 25 hits of the sliding window were recorded) does not coincide with the time variable t , and therefore, the time instant $(t_f - \tau) = 4$ s corresponds to an actual time interval $3.1 \text{ s} < (t_f - \tau) < 4.9 \text{ s}$. It is worth observing that the phase of intensively increasing acoustic activity is again governed by the power law of Eq. (1). The value of the exponent m_1 providing best fit is now equal to $m_1 = 1.05$. Comparing Fig. 5a and b, it becomes clear that the PSC technique provides a warning signal about upcoming fracture earlier than the AE technique.

Coming now to the Dionysos marble beams (recall that they were notched at their mid-span), the time evolution of the PSC for a representative specimen is plotted in Fig. 6a against the $(t_f - t)$ parameter, in juxtaposition to the respective evolution of the normalized load, L/L_f , applied. It is observed that for the time interval $(t_f - t) > 25$ s (or equivalently for load levels not exceeding 98% of the fracture force) the PSC exhibits almost negligible increase from about 1

pA to about 2 pA. From this time instant on (i.e., from $(t_f - t) = 25$ s or $L > 0.98L_f$), the PSC starts increasing quite abruptly attaining a maximum value equal to about 10 pA, almost 1.5 s before the fracture of the beam. During the time interval of its intensive increase, the PSC is excellently governed by the law of Eq. (2) and the corresponding value of the m_2 exponent providing best fit is equal to $m_2 = 0.82$. An enlarged view of the last 10 s of the specific test is shown in Fig. 6b. It is here recalled that displacement-control conditions were adopted for this class of tests. The load exhibits its maximum value about 1.5 s before the macroscopically visible fracture of the specimen, exactly at the time instant at which the PSC exhibits, also, its peak value.

For the same as above test, the number of AE hits, of amplitude exceeding 40 dB, recorded was relatively low, equal to $n = 170$. In this context the number N of AE hits of the sliding window was set equal to $N = 10$. The time evolution of the F-function for this test is plotted in Fig. 6c,

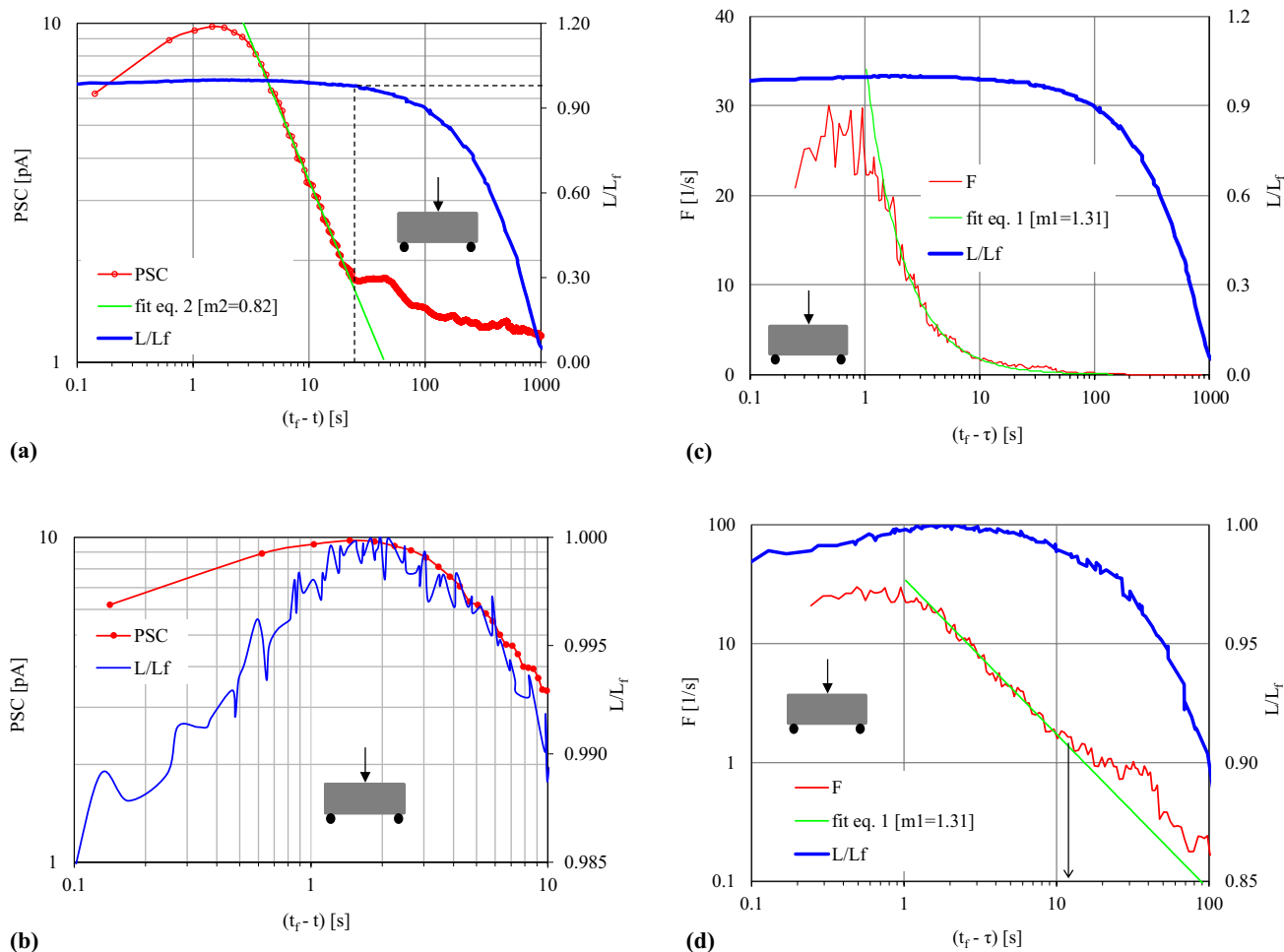


Fig. 6 **a** The PSC in terms of the time-to-failure parameter along logarithmic scales for a marble beam under three-point bending in juxtaposition to the normalized load induced; **b** enlarged view of Fig. 6a for the last 10 s before fracture; **c** the F-function in terms of the time-

to-failure parameter along a semi-logarithmic scale for a marble beam under three-point bending; **d** enlarged view of Fig. 6c for the last 100 s before fracture

in the same way that Fig. 6a is plotted. It is observed from Fig. 6c (and even more clearly from Fig. 6d in which an enlarged view of the last 100 s of the specific test is shown) that during the time interval $1 \text{ s} < (t_f - \tau) < 13 \text{ s}$, the F-function exhibits an abrupt increasing tendency. During this time interval, the F-function obeys excellently the law of Eq. (1) with an m_1 exponent equal to $m_1 = 1.31$. At the time instant with $(t_f - \tau) \sim 1 \text{ s}$, the F-function attains its peak value and then it starts decreasing, however, with strong fluctuations, attributed mainly to the small number of the AE hits recorded.

In full accordance with the conclusions for the intact cement-mortar beam, direct comparison of Fig. 6a and d indicates that the onset of intense increase of the PSC values precedes the respective onset of intense increase of the F-function: the PSC starts increasing abruptly about 25 s before the fracture of the beam while the F-function starts increasing abruptly about 13 s before the fracture of the beam. In other words, the PSC technique provides its pre-failure indicator earlier in comparison to the AE technique.

Again, the electric activity recorded in the cement-mortar beam is stronger (it attains values exceeding 20 pA) than the respective activity in the marble beam (the maximum PSC-value attained does not exceed 10 pA). Moreover, the level of the PSCs recorded is significantly lower compared to the corresponding one recorded during the compression tests. This fact is well documented in the literature (Kyriazopoulos et al. 2011) and is attributed to the significantly smaller portion of the specimen's volume that is activated due to the way the mechanical load is applied during the two tests.

3.3 Direct Tension of Dionysos Marble DENT Specimens

Concerning the sensing setup, the main difference of this protocol (compared to the previous two ones) is that the

electric activity was recorded using two electric sensors (two pairs of electric contacts). Similarly, the acoustic activity was recorded using six acoustic sensors, however, only the data from the two sensors attached in the immediate vicinity of the crowns of the two notches were taken into account in this study. Using two electric and two acoustic sensors was considered necessary to enlighten the response of each one of the two notches (from which macroscopic fracture is expected to start propagating).

The time evolution of the displacement induced and of the respective force developed (recall that this protocol is implemented under displacement-control conditions, at a constant rate) for a typical test is shown in Fig. 7. Fracture occurred at a time instant $t_f = 3008 \text{ s}$, as it was suggested by the fact that at the specific time instant one of the acoustic sensors recorded a hit with amplitude equal to 99 dB. Right after, the other sensor recorded, also, hit of amplitude equal to 99 dB. The maximum load was observed at $t_{L,\max} = 3002 \text{ s}$ and its value was equal to 6251 N (see the plot embedded in Fig. 7).

Starting from the electric activity, the time evolution of the PSCs (denoted as PSC-L and PSC-R for the currents recorded by the sensors eL and eR, i.e., close to the crowns of the left and the right notch, respectively) are plotted in Fig. 8a against the $(t_f - t)$ parameter. In the same figure, the time evolution of the load, L , applied, normalized over its maximum value, L_f , is, also, plotted. The plots of both PSCs are increasing very slowly for the major fraction of the test's duration (i.e., for $20 \text{ s} < (t_f - t) < 3008 \text{ s}$). Then, at the time instant $(t_f - t) = 20 \text{ s}$, i.e., 20 s before fracture, the PSC-L, starts increasing steeply. This steep increase is terminated at the time instant $(t_f - t) \sim 1 \text{ s}$, or in other words about 1 s before macroscopic fracture. The PSC-R, i.e., that recorded by the sensor close to the crown of the right notch, starts increasing steeply at the time instant $(t_f - t) = 7 \text{ s}$, i.e., 7 s before macroscopic fracture. Again,

Fig. 7 The time evolution of the axial displacement in juxtaposition to that of the axial load (displacement-control conditions) for a typical test with a marble specimen under direct tension. The embedded plot displays the very last seconds before fracture

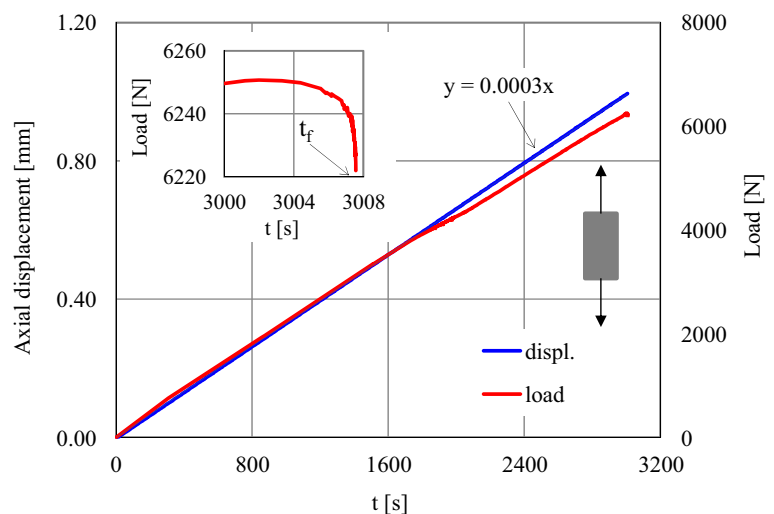
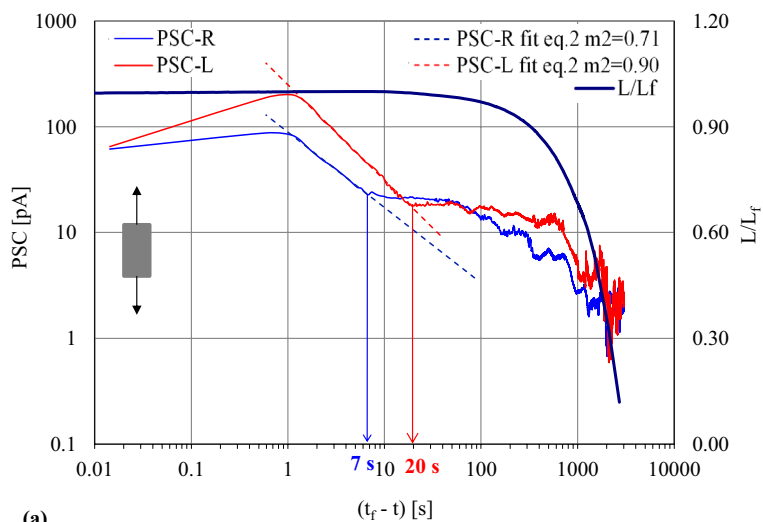
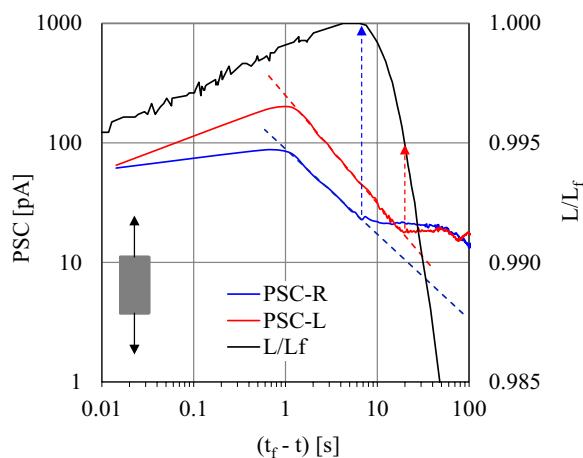


Fig. 8 a The PSC in terms of the time-to-failure parameter along logarithmic scales for a marble specimen under direct tension in juxtaposition to the normalized load induced; **b** enlarged view of Fig. 8a for the last 100 s before fracture



(a)



(b)

this step increase is terminated about 1 s before the fracture of the specimen.

Comparative consideration of PSC-L and PSC-R indicates that:

- (i) The onset of the step increase of the PSC-R is recorded approximately 13 s later than the corresponding increase of the PSC-L. In terms of the load applied, the onset of step increase of PSC-L is observed for $L/L_f \sim 0.995$ while that of the PSC-R for $L/L_f \sim 1$ (see Fig. 8b, in which an enlarged view of the plots of Fig. 8a is shown for the last 100 s of the test's duration).
- (ii) The electric signal recorded by the sensor close to the crown of the left notch, i.e., PSC-L, is significantly stronger compared to the PSC-R. The maximum value attained by PSC-L is equal to about 200 pA while the respective maximum value attained by PSC-R is equal to only 80 pA.

Both observations are in agreement with the fact (observed by means of a high-speed camera) that the fracture for the specific test started propagating from the crown of the left notch towards that of the right notch implying that damage mechanisms activated around the crown of the left notch are more intense compared to those activated around the crown of the right notch. Given that the electric signal is directly related to the level of internal damage, it should be expected that the PSC-L signal is stronger compared to the PSC-R one.

What is, however, more important for the target of the present study is that, for both the PSC-L and the PSC-R, the phase of step increase of the evolution of the electric activity is perfectly described by the power law of Eq. (2). The values for the exponent m_2 are equal to $m_2 = 0.90$ and $m_2 = 0.71$ for the PSC-L and the PSC-R, respectively.

Concerning the respective acoustic activity in the specific specimen, the two acoustic sensors, chL and chR (denoted in accordance with the notation adopted for the electric

sensors) recorded $n = 317$ and $n = 216$ acoustic hits, respectively, of amplitude exceeding 40 dB. In this context, the function F was now calculated using a sliding window with $N = 20$ successive hits. The time evolution of the F -functions, as determined by the data of the two acoustic sensors, is plotted in Fig. 9a (again in juxtaposition to the normalized load applied), against the time-to-failure parameter along semi-logarithmic scale. It is obvious that the acoustic activity recorded by the sensor close to the crown of the left notch (chL) is significantly stronger compared to that recorded by the chR sensor. Moreover, the onset of steeply increasing values of the F -function obtained from the data of the chL sensor precedes that of the chR one, in full accordance with the respective observations for the electric activity.

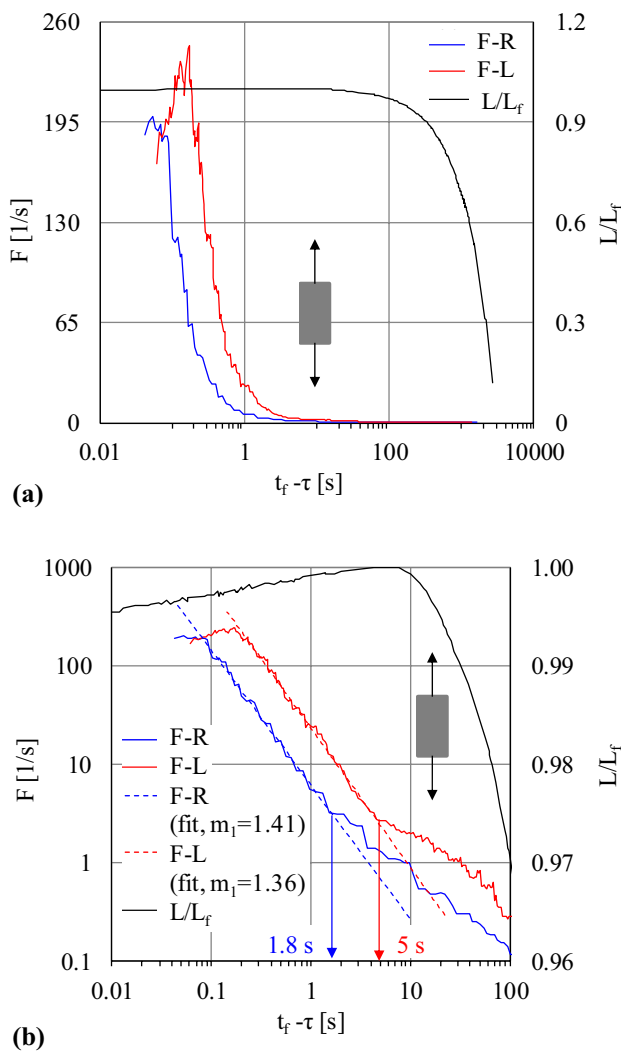


Fig. 9 **a** The F -function in terms of the time-to-failure parameter along a semi-logarithmic scale for a marble specimen under direct tension in juxtaposition to the normalized load induced; **b** enlarged view of Fig. 9a for the last 100 s before fracture

In an attempt to gain clearer insight into the acoustic activity during the very last loading stages, attention is focused to the time interval $0.01 \text{ s} < (t_f - \tau) < 100 \text{ s}$, and the respective plots of the F -function and the load applied are shown in Fig. 9b (pay attention that in Fig. 9b the scale of the F -functions is also logarithmic). It is seen from Fig. 9b that for the F -function of the chL sensor the steep increase starts at $(t_f - \tau) \approx 5 \text{ s}$. Recalling that the value $(t_f - \tau) \approx 5 \text{ s}$ is the average value of $N = 20$ time instants, it can be calculated that the specific time instant corresponds to a time interval with $2 \text{ s} < (t_f - t) < 9 \text{ s}$. Taking into account that the steep increase of the PSC started at $(t_f - t) = 20 \text{ s}$, it is again indicated that the PSC signal provides earlier (compared to the signal of the AE technique) a warning (pre-failure indicator) about upcoming macroscopic fracture. Similarly, it is seen from Fig. 9b, that the onset of steep increase for the F -function of the chR sensor starts at $(t_f - \tau) \approx 1.8 \text{ s}$ corresponding to a time interval $0.4 \text{ s} < (t_f - t) < 6 \text{ s}$ while the steep increase of the PSC-R was detected at $(t_f - t) = 7 \text{ s}$.

Again, the time evolution of the F -function for both acoustic sensors during the phase of its steep increase is governed by the power law of Eq. (1) (see Fig. 9b) and the values of the m_1 exponent are equal to $m_1 = 1.36$ and $m_1 = 1.41$, for the chL and the chR sensors, respectively.

4 Discussion

In this study, advantage was taken of series of well-known experimental observations that subjecting specific classes of building materials to mechanical loads, at levels leading to the formation and propagation of networks of micro-cracks, results to various types of emissions, including among others thermal, acoustic and electromagnetic ones (Courtney 2005; De Groot et al. 1995; Dickinson et al. 1981; Giordano et al. 1998; Surkov and Hayakawa 2014). These emissions have been long ago considered by structural engineers as potential tools for Structural Health Monitoring (SHM) purposes (Evans and Linzer 1973; Jones 2008; Mohammad and Huang 2010; Ramirez-Jimenez et al. 2004; Sauce 2016). A detailed review of the sensing techniques based on electromagnetic emission phenomena, including, also, applications for Structural Health Monitoring purposes, was very recently published by Sharma et al. (2021).

In this direction, special attention has been paid long ago to the weak electric signals (usually denoted as Pressure-Stimulated Currents) produced while specific classes of materials, both piezoelectric and nonpiezoelectric, are loaded mechanically. One could mention, for example, Whitworth's (1975) pioneering work in alkali halides, dated back to 1975. In fact, there are quite a few works dealing with the specific kind of emissions both from the theoretical and the experimental points of view. In general, it is

accepted that the phenomenon is associated with the development of microcracks in quasi-brittle, nonmetallic materials which produce electric charges due to the formation of electric dipoles. As it was mentioned, these dipoles constitute charged systems (Varotsos et al. 2002), producing an electric potential across the crack which is responsible for electric current flow. It is to be emphasized here, that the detection of these electric currents is potentially a precursor of large-scale fracture phenomena since, besides the laboratory level, they have been also measured at geodynamic scales (Varotsos 2005). The current scientific challenge is the verification of the applicability of the laboratory findings to the understanding of mega-scale phenomena such as, for example, field observations of electric earthquake precursors (Varotsos 2005).

Concerning, now, the physical interpretation of this kind of emissions, a comprehensive review, discussing available models was published recently by Saltas et al. (2018). It is to be accepted from the very beginning, that various electrification mechanisms have been proposed to explain the emission of these very weak transient electric currents, produced when specimens made of rocks and rock-like materials are loaded mechanically at stress level approaching the one causing macroscopic fracture. They are commonly attributed to the generation, opening, coalescence and propagation of microcracks within the mass of the material (Bleier et al. 2010; Freund 2002; Lavrov 2005). These electrification mechanisms, induced by micro-fracturing processes, include:

- Electrokinetic effects due to the water flow in permeable rocks (in this case, gravity and crustal strain are the driving forces),
- Activation of positive holes in quartz-free rocks,
- Piezoelectricity in quartz-bearing rocks,
- Flowing gases,
- Motion of conductive earth materials (here, the driving force is the acoustic waves), and
- Motion of charged dislocations (MCDs).

The efficiency of each one of the above-mentioned mechanisms is still under intensive investigation by many researchers worldwide and no definite, generally accepted, theory is as yet available. It could be stated, for example, that an explanation in terms of the “activation of positive holes in quartz-free rocks” (Takeuchi et al. 2011, 2013) is applicable for the materials tested in the protocols described in the present study. Indeed, Takeuchi et al. (2011; 2013) taking advantage of data obtained from experiments with gabbro (which almost contains no free-quartz crystals with a porosity less than 1%) specimens, provided interesting experimental evidence supporting this explanation. Again,

however, it seems that this is an assumption rather than actual observation.

Besides the above model based on the “activation of positive holes in quartz-free rocks”, the MCD model, originally proposed by Slifkin (1993) and further developed by Vallianatos and Tzanis (1999) is, also, widely accepted, since it is associated with brittle fracture in both piezoelectric and nonpiezoelectric rocks. A synoptic description of the basic principles of this model, together with an analytic discussion, was presented by Vallianatos et al. (2004). According to the MCD model, the transient electric currents recorded are related to the nonstationary accumulation of deformation. For the case of elastic deformation of the sample, the strain rate is obviously proportional to the stress rate. Assuming that the PSC is proportional to the strain rate, it is implied that for specimens under constant stress rate, it is not expected to observe any transient PSC effect, as long as the loading level remains within the elastic region. On the contrary, when the stress level exceeds the elastic limit and non-reversible damage mechanisms are activated (i.e., networks of microcracks are formed and propagate), Young’s modulus does not remain constant and the strain rate starts increasing. As a result, it is expected that the magnitude of the PSC will start increasing. The MCD model was found to be in accordance with findings of laboratory tests with specimens made of dried marble, subjected to uniaxial loading under various loading schemes by Vallianatos et al. (2004). Data of a typical example, in which Dionysos marble specimens were subjected to uniaxial compression under constant displacement rate, equal to 5×10^{-4} mm/s, are plotted in Fig. 10, in which the time evolution of the normalized (over the maximum value attained) axial stress is plotted in juxtaposition to the respective evolution of the PSC recorded. Four intervals can be clearly distinguished. The first one ($0 < t < 550$ s), denoted as I in Fig. 10, is characterized by a weak maximum of the PSC, at very low stress level ($0 < \sigma/\sigma_{\max} < 0.2$). In

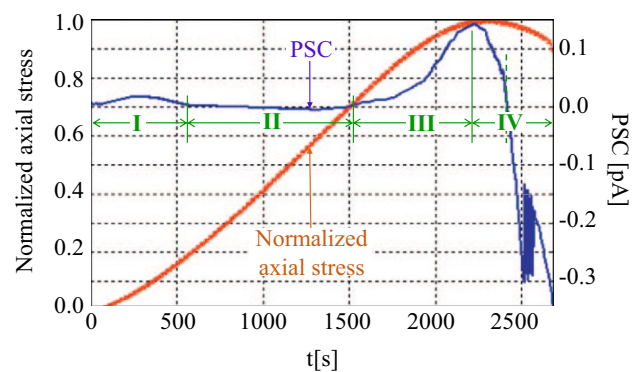


Fig. 10 Time evolution of the normalized axial stress (orange line) in juxtaposition to that of the PSC recorded (blue line) for a Dionysos marble specimen subjected to uniaxial compression under constant displacement rate (Vallianatos et al. 2004)

terms of Rock Mechanics findings, this weak PSC maximum (associated with increasing elastic modulus) could be attributed to pore-closing processes. Then, when the applied stress is within the linear elastic region, denoted as II in Fig. 10 ($550 \text{ s} < t < 1520 \text{ s}$), the electric activity vanishes almost completely, in accordance with the expected reversible nature of the phenomena within the linear elastic region of the stress–strain curve. After the material abandons its linear elastic behavior, i.e., in interval III ($1520 \text{ s} < t < 2200 \text{ s}$), the PSC starts increasing steadily towards a maximum value (which is attained a little before the applied stress reaches its own maximum value) due to the activation of damage mechanisms, mainly in the form of generation of networks of microcracks. Finally, the PSC starts decreasing due to sequential and continuous development of macro-cracks which reduce the electric paths. The strong fluctuations of the PSC observed during the very last loading steps, as well as its polarity reverse, are still under discussion. An example of a protocol during which electric currents have been recorded at load levels well below the proportionality limit (i.e., within the region considered (macroscopically) as perfectly elastic with reversible phenomena) was described by Vallianatos et al. (2004): cubic Dionysos marble specimens were subjected to stepwise uniaxial compression, at stress levels between 3 and 12 MPa (i.e., below 20% of the compressive strength of Dionysos marble (Kourkoulis et al. 1999)). The time evolution of the axial stress imposed is plotted in Fig. 11a, while the time evolution of the stress rate, $d\sigma/dt$, is plotted in Fig. 11b (dotted line) in juxtaposition to the respective evolution of the PSC recorded (continuous line). It is seen from Fig. 11 that when the stress rate is constant, i.e., portions AB of the stress in Fig. 11a, b, the PSC recorded attains very low, almost constant values (portion A'B' in Fig. 11b), as it is indeed predicted by the MCD model. However, when the stress rate ceases being constant (either increasing or decreasing, i.e., portions BC in Fig. 11a, b), the PSC starts increasing towards a maximum value (point P' in Fig. 11b) and then it decreases towards its initial level (portion B'P'D' in Fig. 11b). A possible explanation for the specific observation could be provided taking into account that the load level applied in the specific protocol is within the pore-closing regime of the stress–strain curve (indeed, according to Fig. 10, this pore-closing region is observed at stress levels equal to about 10% of the ultimate compressive strength of Dionysos marble). Given that the compressive strength of this material varies around 75 MPa the stress level imposed in Fig. 11a seems to correspond to the pore-closing regime.

Recapitulating, it could be stated that in spite of the intensive research efforts devoted to the topic and the fact that the above-mentioned sensing techniques (based on the weak electric emissions undoubtedly observed experimentally) are widely adopted and used for practical purposes

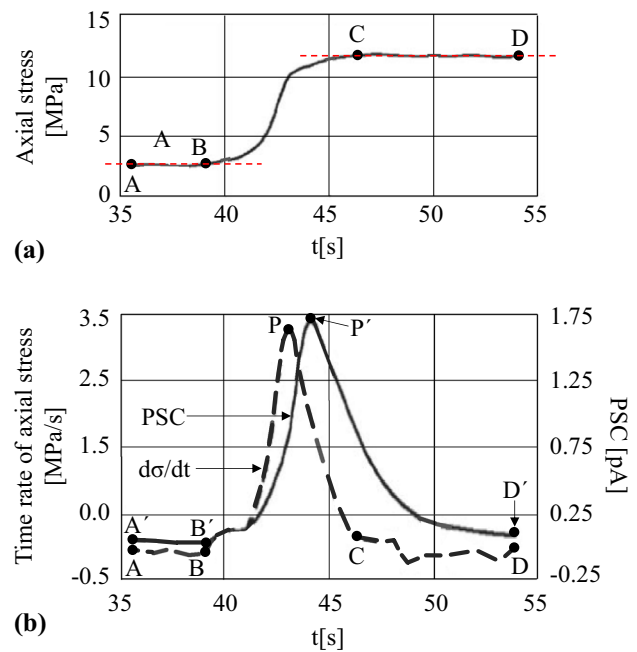


Fig. 11 **a** Time evolution of the stress applied and **b** time evolution of the stress rate (dotted line) and the PSC recorded (continuous line), during uniaxial compression of a Dionysos marble specimen under a stress-control loading scheme at relatively low load levels (in comparison to the ones causing fracture of the specific marble variety) (Vallianatos et al. 2004)

(for a broad variety of building materials), there is still a long way until a proper understanding of the underlying mechanisms generating these emissions is achieved (especially in case more than one mechanisms are activated simultaneously).

Before concluding the discussion devoted to the PSCs, it should be mentioned that, in general, the polarity of the PSCs recorded is not always positive. For the sake of simplicity, in case the PSC recorded on a specific channel is of single polarity then this information is omitted (using the absolute values of the PSCs) since it is believed that it does not add any kind of useful information. For completeness reasons, however, it is here clarified that experimental protocols are mentioned in the literature, where changes of the polarity were observed and discussed (Saltas et al. 2018; Stavarakas et al. 2003; Vallianatos et al. 2004). Although a final explanation is not as yet available, it is believed that the polarity of the recorded PSC is related to the direction of the crack propagation, in accordance with the most dominant, up to now, physical interpretation of the PSCs (i.e., the Moving Charged Dislocation model already discussed in previous paragraphs). The authors' team is currently working in this direction, collecting large data sets, where grids of sensors are used (Stavarakas et al. 2019) and different polarities are recorded, in an attempt

to study the influence of the direction of the fracture plane formation on the PSC polarity.

5 Concluding Remarks

Data from three different experimental protocols, including monotonic mechanical loading up to fracture, were assessed in this study, aiming to reveal hidden affinities between the electric and acoustic activities, developed within the loaded specimens, at load levels close to these causing macroscopic fracture. In addition, the study aimed to reveal possible pre-failure indicators that are provided by the data recorded using both a mature and well-founded sensing technique (i.e., that of the Acoustic Emissions) and, also, a relatively recently introduced one, i.e., that of the Pressure-Stimulated Currents. Besides the potentially interesting conclusions drawn, the innovation of the study lies in the use of data obtained from different loading schemes (compression, 3PB and tension), different materials (cement mortar and Dionysos marble), different specimens (notched and intact) and different load application protocols (displacement- and load-control conditions). The broad variety of data considered in this study offers quite a reliable support to the conclusions drawn, while at the same time, it is indicated that perhaps it could be used, also, for engineering purposes, assuming, of course, that practical problems related, for example, to the magnitude of the electric currents recorded with respect to the inevitable electromagnetic “noise” will be resolved.

In this study, the electric activity was assessed in terms of the Pressure-Stimulated Currents while the acoustic activity was assessed in terms of the F-function (Triantis and Kourkoulis 2018). At this point, one should comment on the numerical value of N (i.e., the number of successive hits included in the sliding window used to calculate the F-function), which represents the “resolution” of the analysis and its choice appears to be somehow arbitrary. In fact, the value of N to be chosen depends on the overall number of hits that are recorded during the test: Increased number of total hits permits choosing a high value for N and vice versa. In a previous study, it was proven that the value of N does not significantly influence the results of the analysis, assuming that N is a small fraction of the total number of hits (Triantis and Kourkoulis 2018).

For all three protocols, it was concluded that both the electric and the acoustic activities are very weak during the major part of the loading procedure. It is only during the very last loading stages that they are strongly intensified. Moreover, for the compression tests (first protocol), it was indicated that the onset of steep increase of the F-function and of the PSC is directly related to the time instant at which the mechanical response of the materials

studied (in terms of their axial stress—axial strain relation) abandons linearity. Equivalently, it could be said that the strong intensification of the acoustic and electric activities is directly related to the onset of generation of non-reversible phenomena within the mass of the specimen tested.

Concerning the compression and 3PB experimental protocols, in which cement-mortar and marble specimens were tested, it was noted that the electric activity in the cement-mortar specimens is significantly stronger compared to the respective activity in marble specimens.

Regarding the protocol with the DENT specimens (i.e., specimens with two potential fracture initiation areas), the electric and acoustic signals recorded by the sensors close to the crown from which fracture started are systematically stronger compared to the respective activities around the crown of the other notch (i.e., the notch towards which fracture is propagating).

Moreover, it was concluded that, for all three experimental protocols, both the AE- and the PSC-techniques provide well distinguishable indicators (i.e., the onset of rapid increase of either the F-function or the values of the PSC), warning about upcoming catastrophic fracture. At this point, it is worth emphasizing that in some cases, the onset of rapid increase of the PSC values precedes the respective onset of rapid increase of the F-function. In other words, it could be stated that sometimes the PSC technique provides earlier its pre-failure indicator with respect to the AE technique. It could be anticipated at this point that this depends on the choice of the arbitrary value of N . However, this is by no means the case. In a recent study, Triantis and Kourkoulis (2018) considered in-depth the specific issue. It was definitely concluded that “... the value of N somehow describes the “resolution” of the analysis. Fortunately, the exact numerical value assigned to N does not significantly influence the results of the analysis, assuming of course that N is a relatively small fraction of the total number of hits recorded during the test’s duration”. The specific condition is clearly fulfilled in the present analysis and therefore one could safely state that the conclusions drawn do not depend on the specific choice of the value of N . Moreover, the fact that the PSC appears providing its pre-failure indicators somehow earlier, in comparison to the respective ones of the AEs, is observed, also, when the acoustic activity is analyzed in terms of the I_b -value or the energy released, rather than in terms of the F-function, i.e., in terms of parameters calculated without the need to arbitrarily predefine a number N of hits (Pasiou and Triantis 2017).

In addition, for the direct tension tests of double-edge notched specimens, the electric and the acoustic activities, recorded by the sensors attached close to the crown of the notch from which fracture starts, provide the respective

Table 1 The values of the m_1 and m_2 exponents of the power laws of Eqs. (1) and (2)

| Material → Experiment ↓ | Marble | | | Cement mortar | | |
|----------------------------|------------|---------|---------|---------------|---------|---------|
| | Specimen ↓ | m_1 ↓ | m_2 ↓ | Specimen ↓ | m_1 ↓ | m_2 ↓ |
| Compression | Intact | 1.20 | 1.04 | Intact | 0.84 | 0.71 |
| 3PB | Notched | 1.31 | 0.82 | Intact | 1.05 | 0.91 |
| DENT (left notch) | Notched | 1.36 | 0.90 | | | |
| DENT (right notch) | Notched | 1.41 | 0.71 | | | |

pre-failure indicators earlier, with respect to the indicators provided by the sensors attached at the crown of the other notch. Moreover, the latter indicators are significantly weaker.

Finally, it was concluded that for all three protocols and during the time interval of intense increase of the acoustic and the electric activity (i.e., after the pre-failure warning signals are emitted), the F-function and the PSC are governed by a power law, assuming that their time evolution is expressed in terms of the time-to-failure parameter. The values of the exponents of this law [Eqs. (1) and (2)], which could be considered as representing the intensity of increase of the acoustic and electric activities, vary in the $0.71 < (m_1, m_2) < 1.41$ range, as it is seen in Table 1. It is here clarified that the author's team is not as yet in the position to discuss on whether these parameters should vary within a narrower interval or not. The topic is to be studied further with a wider variety of materials and loading schemes. In general, experiments with specimens made of rocks and rock-like materials exhibit, by default, wide scattering due to their varying composition and layered structure. Moreover, it is mentioned that a variety of loading schemes were implemented in the present study together with specimens of varying geometries and dimensions. For the moment being, it is not clear whether these factors influence (and to what extent) the values of the m_1 and m_2 exponents and the relative study is in progress.

The specific power law mentioned in previous paragraph was recently found to govern the acoustic activity, also, for protocols including stepwise rather than monotonic loading (Triantis et al. 2019). However, it is the first time that such a law was found to govern, also, the evolution of the electric signals (expressed in terms of the PSCs), providing another strong correlation between the outcomes of the AE- and PSC-techniques. It is hoped that the conclusions drawn from the present study will be valuable for the ongoing attempt to quantitatively calibrate the outcomes of the PSC technique versus the respective ones of mature sensing techniques, like that of the AEs. This is one of the most crucial steps (together with that concerning the detection and location of the critical areas where fracture is expected by means, perhaps, of a grid of electric sensors instead of a single one) before the PSC technique could be proposed as an undoubtedly reliable

Structural Health Monitoring tool, in terms of the time evolution of the electric current recorded, i.e., in terms of the (PSC-t) plots.

Declarations

Conflict of Interest All the authors declare no conflicts of interest.

References

- Aggelis DG, Mpalaskas A, Matikas TE (2013) Acoustic signature of different fracture modes in marble and cementitious materials under flexural load. *Mech Res Commun* 47:39–43
- Archer JW, Dobbs MR, Aydin A, Reeves HJ, Prance RJ (2016) Measurement and correlation of acoustic emissions and pressure stimulated voltages in rock using an electric potential sensor. *Int J Rock Mech Min* 89:26–33
- Aydin A, Prance RJ, Prance H, Harland CJ (2009) Observation of pressure stimulated voltages in rocks using an electric potential sensor. *Appl Phys Lett* 95:124102
- Bleier T, Dunson C, Alvarez C, Freund F, Dahlgren R (2010) Correlation of pre-earthquake electromagnetic signals with laboratory and field rock experiments. *Nat Hazards Earth Syst Sci* 10(9):1965–1975
- Cartwright-Taylor A, Vallianatos F, Sammonds P (2014) Superstatistical view of stress-induced electric current fluctuations in rocks. *Physica A* 414:368–377
- Courtney TH (2005) *Mechanical behavior of materials*, 2nd edn. Wiley, USA
- De Groot PJ, Wijnen PA, Janssen RB (1995) Real-time frequency determination of acoustic emission for different fracture mechanisms in carbon/epoxy composites. *Compos Sci Technol* 55(4):405–412
- Dickinson J, Donaldson E, Park M (1981) The emission of electrons and positive ions from fracture of materials. *J Mater Sci* 16(10):2897–2908
- Eitzen DG, Wadley HNG (1984) Acoustic emission: establishing the fundamentals. *J Res Nat Bur Stand* 89:75–100
- Enomoto J, Hashimoto H (1990) Emission of charged particles from indentation fracture of rocks. *Nature* 346:641–643
- Evans AG, Linzer M (1973) Failure prediction in structural ceramics using acoustic emission. *J Am Ceram Soc* 56(11):575–581
- Exadaktylos GE, Vardoulakis I, Kourkoulis SK (2001) Influence of nonlinearity and double elasticity on flexure of rock beams – II. Characterization of Dionysos marble. *Int J Solids Struct* 38(22–23):4119–4145
- Freund F (2002) Charge generation and propagation in igneous rocks. *J Geodyn* 33:543–570

- Fursa TV, Dann DD, Petrov MV, Lykov AE (2017) Evaluation of damage in concrete under uniaxial compression by measuring electric response to mechanical impact. *J Nondestruct Eval* 36(2):30
- Fursa TV, Petrov M, Dann DD, Reutov YA (2019) Evaluating damage of reinforced concrete structures subjected to bending using the parameters of electric response to mechanical impact. *Compos Part B-Eng* 158:34–45
- Giordano M, Calabro A, Esposito C, Damore A, Nicolais L (1998) An acoustic-emission characterization of the failure modes in polymer-composite materials. *Compos Sci Technol* 58(12):1923–1928
- Ishida T, Labuz JF, Manthei G, Meredith PG et al (2017) ISRM suggested method for laboratory acoustic emission monitoring. *Rock Mech Rock Eng* 50:665–674
- Jones MA (2008) Structural-health monitoring: A sensitive issue. *Nat Photonics* 2(3):153–154
- Kleftakis S, Agioutantis Z, Stiakakis C (2000) Numerical simulation of the uniaxial compression test including the specimen-platen interaction. Proc. 4th Int. Colloquium on Computation of Shell and Spatial Structures IASS-IACM, Jun 4–7, 2000, Chania, Greece
- Kourkoulis SK, Exadaktylos GE, Vardoulakis I (1999) U-notched Dionysos-Pentelicon marble in three point bending: the effect of non-linearity, anisotropy and microstructure. *Int J Fracture* 98(3–4):369–392
- Kourkoulis SK, Pasiou ED, Dakanali I, Stavrakas I, Triantis D (2018) Notched marble plates under tension: detecting pre-failure indicators and predicting entrance to the “critical stage.” *Fatigue Fract Eng M* 41:776–786
- Kyriazopoulos A, Anastasiadis C, Triantis D, Brown CJ (2011) Non-destructive evaluation of cement-based materials from pressure-stimulated electrical emission—Preliminary results. *Constr Build Mater* 25:1980–1990
- Lavrov A (2005) Fracture-induced physical phenomena and memory effects in rocks: a review. *Strain* 41:135–149
- Li Z, Wang E, He M (2015) Laboratory studies of electric current generated during fracture of coal and rock in rock burst coal mine. *J Mining*. 2015:235636
- Loukidis A, Triantis D, Stavrakas I, Pasiou ED, Kourkoulis SK (2021) Comparative Ib-value and F-function analysis of Acoustic Emissions from elementary and structural tests with marble specimens. *Mater Des Process Commun* 3:e176
- Mohammad I, Huang H (2010) Monitoring fatigue crack growth and opening using antenna sensors. *Smart Mater Struct* 19(5):055023
- Niu Y, Zhou XP, Zhou LS (2019) Fracture damage prediction in fissured red sandstone under uniaxial compression: acoustic emission b-value analysis. *Fatigue Fract Eng Mater Struct* 43:175–190
- Ogawa TK, Miura T (1985) Electromagnetic radiation from rocks. *J Geophys Res* 90:6245–6249
- Ohtsu M (2010) RILEM TC 212-ACD: acoustic emission and related NDE techniques for crack detection and damage evaluation in concrete. *Mater Struct* 43:187–1189
- Pasiou ED, Triantis D (2017) Correlation between the electric and acoustic signals emitted during compression of brittle materials. *Fracture Struct Integrity* 40:41–51
- Ramirez-Jimenez C, Papadakis N, Reynolds N, Gan T, Purnell P, Pharaoh M (2004) Identification of failure modes in glass/polypropylene composites by means of the primary frequency content of the acoustic emission event. *Compos Sci Technol* 64(12):1819–1827
- Saltas V, Vallianatos F, Triantis D, Stavrakas I (2018) Complexity in laboratory seismology: from electrical and acoustic emissions to fracture. In: complexity measurement and application to seismic time series, measurement and application, Elsevier, Ch 8, pp 239–273
- Sause MGR (2016) In situ monitoring of fiber-reinforced composites. *Springer Ser Mater Sci* 2016:242
- Sharma SK, Sivarathri AK, Chauhan VS, Sinapius M (2018) Effect of low temperature on electromagnetic radiation from soft PZT SP-5A under impact loading. *J Electron Mater* 47(10):5930–5938
- Sharma SK, Chauhan VS, Sinapius M (2021) A review on deformation-induced electromagnetic radiation detection: history and current status of the technique. *J Mater Sci* 56:4500–4551
- Slifkin L (1993) Seismic electric signals from displacement of charged dislocations. *Tectonophysics* 224:149–152
- Stavrakas I, Anastasiadis C, Triantis D, Vallianatos F (2003) Piezo stimulated currents in marble samples: precursory and concurrent-with-failure signals. *Nat Hazard Earth Syst Sci* 3:243–247
- Stavrakas I, Kourkoulis SK, Triantis D (2019) Damage evolution in marble under uniaxial compression monitored by Pressure Stimulated Currents and Acoustic Emissions. *Fracture Struct Integrity* 50:573–583
- Stavrakas I, Triantis D, Agioutantis Z, Maurigiannakis S, Saltas V, Vallianatos F (2004) Pressure Stimulated Currents in rocks and their correlations with mechanical properties. *Nat Hazards Earth Syst Sci* 4:563–567
- Surkov V, Hayakawa M (2014) Laboratory study of rock deformation and fracture ultra and extremely low frequency electromagnetic fields. Springer Geophysics, Japan, pp 335–372
- Takeuchi A, Nagao T (2013) Activation of hole charge carriers and generation of electromotive force in gabbro blocks subjected to nonuniform loading. *J Geophys Res Solid Earth* 118(3):915–925
- Takeuchi A, Aydan Ö, Sayanagi K, Nagao T (2011) Generation of electromotive force in igneous rocks subjected to non-uniform loading. *Earthq Sci* 24(6):593–600
- Triantis D, Kourkoulis SK (2018) An alternative approach for representing the data provided by the acoustic emission technique. *Rock Mech Rock Eng* 51:2433–2438
- Triantis D, Stavrakas I, Anastasiadis C, Kyriazopoulos A, Vallianatos F (2006b) An analysis of Pressure Stimulated Currents (PSC), in marble samples under mechanical stress. *Phys Chem Earth* 31:234–239
- Triantis D, Anastasiadis C, Stavrakas I (2008) The correlation of electrical charge with strain on stressed rock samples. *Nat Hazard Earth Syst* 8:1243–1248
- Triantis D, Stavrakas I, Kyriazopoulos A, Hloupis G, Agioutantis Z (2012) Pressure stimulated electrical emissions from cement mortar used as failure predictors. *Int J Fracture* 175:53–61
- Triantis D, Stavrakas I, Pasiou ED, Kourkoulis SK (2020) Assessing the acoustic activity in marble specimens under stepwise compressive loading. *Mat Design Process Comm* 100:1–7
- Triantis D, Anastasiadis C, Stavrakas I, Kyriazopoulos A (2006) The ascertainment of the presence of damage processes using the pressure stimulated current (PSC) technique on marble and cement samples. Proc. 9th ECNDT, Tu.1.6.2, Sept 25–29, 2006, Berlin, Germany
- Vallianatos F, Tzani A (1999) On possible scaling laws between electric earthquake precursors (EEP) and earthquake magnitude. *Geophys Res Lett* 26:2013–2016
- Vallianatos F, Triantis D, Tzani A, Anastasiadis C, Stavrakas I (2004) Electric earthquake precursors: from laboratory results to field observations. *Phys Chem Earth* 29:339–351
- Vardoulakis I, Exadaktylos GE, Kourkoulis SK (1998) Bending of marble with intrinsic length scales: a gradient theory with surface energy and size effects. *J Phys IV* 8:399–406
- Varotsos PA (2005) The Physics of seismic electric signals. TERRAPUB, Tokyo
- Varotsos P, Sarlis N, Lazaridou M, Kapiris P (1998) Transmission of stress induced electric signals in dielectric media. *J Appl Phys* 83(1):60–70
- Varotsos PA, Sarlis NV, Skordas ES (2002) Long-range correlations in the electric signals that precede rupture. *Phys Rev E* 66:011902
- Wang X, Wang E, Liu X (2019) Damage characterization of concrete under multi-step loading by integrated ultrasonic and acoustic emission techniques. *Constr Build Mater* 221:678–690
- Whitworth RW (1975) Charged dislocations in ionic crystals. *Adv Phys* 24:203–304

- Yoshida S, Uyeshima M, Nakatani M (1997) Electric potential changes associated with a slip failure of granite: preseismic and coseismic signals. *J Geophys Res* 102:14883–14897
- Zhang JZ, Zhou XP, Zhou LS, Berto F (2019) Progressive failure of brittle rocks with non-isometric flaws: Insights from acousto-optic-mechanical (AOM) data. *Fatigue Fract Eng Mater Struct* 42:1787–1802

Publisher's Note Springer Nature remains neutral with regard to jurisdictional claims in published maps and institutional affiliations.